Polaronic Aspects of the two-dimensional ferromagnetic Kondo Model

Maria Daghofer,[1] Winfried Koller,[2] Hans Gerd Evertz,[1] and Wolfgang von der Linden[1]

[1]*Institute for Theoretical and Computational Physics, Graz University of Technology, Petersgasse 16, A-8010 Graz, Austria.**

[2]*Department of Mathematics, Imperial College, 180 Queen's Gate, London SW7 2BZ, UK.*

(Dated: December 16, 2003)

The 2D ferromagnetic Kondo model with classical corespins is studied via unbiased Monte-Carlo simulations. A canonical algorithm for finite temperatures is developed. We show that with realistic parameters for the manganites and at low temperatures, the double-exchange mechanism does not lead to phase separation on a two-dimensional lattice but rather stabilizes individual ferromagnetic polarons. A detailed analysis of unbiased MC results reveals that the polarons can be treated as independent particles. It is found that a simple polaron model perfectly describes the physics of the FM Kondo model. The ferromagnetic polaron picture provides an obvious explanation for the pseudogap in the one-particle spectral function $A_k(\omega)$ observed in the FM Kondo model.

PACS numbers: 71.10.-w,75.10.-b,75.30.Kz

I. INTRODUCTION

Manganese oxides such as $La_{1-x}Sr_xMnO_3$, $La_{1-x}Ca_xMnO_3$ and $La_{2-2x}Sr_{1+2x}Mn_2O_7$ have been attracting considerable attention since the discovery of colossal magnetoresistance (CMR)[1,2]. These materials crystallize in the perovskite-type lattice structure where the crystal field breaks the symmetry of the atomic wave function of the manganese d-electrons. The energetically lower t_{2g} levels are occupied and form a localized corespin with $S = 3/2$. The e_g orbitals are hybridized with the neighboring oxygen $2p$ orbitals and electrons can thereby move from one Mn ion to another. Some compounds crystallize in structures with well separated MnO_2-(bi)layers, to which the itinerant e_g electrons are confined. The interplay of various physical ingredients such as the strongly FM Hund coupling (J_H) of the itinerant electrons to localized corespins, AFM Superexchange of the corespins, Coulomb correlations, and electron-phonon coupling leads to a rich phase diagram including antiferromagnetic insulating, ferromagnetic metallic and charge ordered domains. The dynamics of the charge carriers moving in the spin and orbital background shows remarkable dynamical features[3,4].

Since full quantum mechanical many-body calculations for a realistic model, including all degrees of freedom, are not yet possible, several approximate studies of simplified models have been performed in order to unravel individual pieces of the rich phase diagram of the manganites. The electronic degrees of freedom are generally treated by a Kondo lattice model[5]. Electron-electron correlation is often neglected, because the on-site Hubbard term merely renormalizes the already strong Hund coupling. For the Kondo model with quantum spins it is still difficult to derive rigorous numerical or analytical results, especially in dimensions higher than one. If the S=3/2 corespins are treated classically, however, the model can be treated by unbiased Monte Carlo techniques. The validity of this approximation has been tested in Ref. 6,7,8,9 and it appears that quantum effects are important for (S=1/2) corespins or at $T = 0$. For finite temperature and S=3/2, classical spins present a reasonable approximation.

Further approximations can be made by taking into account, that the Hund coupling J_H is much stronger than the kinetic energy. Consequently, configurations are very unlikely in which the electronic spin is antiparallel to the local corespin. A customary approach is to take $J_H \to \infty$. This approximation however breaks down for the almost completely filled lower Kondo band. In the dilute hole regime, the full Kondo model is governed by an effective AFM interaction between the corespins due to excitations into the upper Kondo band. This effect is completely absent from the $J_H \to \infty$ model.

An effective spinless fermion (ESF) model[10] has been proposed to improve upon the $J_H \to \infty$ limit. In this model, virtual excitations account for effects of configurations, where the itinerant electron spin is antiparallel to the local corespin. It has been demonstrated that the results of the ESF model are in excellent agreement with those of the original Kondo model even for moderate values of J_H.

Elaborate Monte Carlo (MC) simulations for the FM Kondo with classical t_{2g} corespins in various dimensions have been performed[9,10,11,12,13,14,15,16,17,18,19,20] in order to unravel the physical properties of the DE model. For a review see for example Ref. 14 and references therein. A two-dimensional Kondo lattice model for manganites has been thoroughly investigated in Ref. 20 by means of MC calculations similar to ours and by analytical energy comparison of several phases. Using a relatively high value for the antiferromagnetic exchange coupling and infinite Hund's rule coupling $J_H \to \infty$, Aliaga *et al* find PS, stripes, island phases for commensurate fillings, and a so called "Flux phase" on the two-dimensional lattice. By island phases, the authors mean small ferromagnetic domains that are stacked antiferromagnetically. In a 2D-Kondo model applied to cuprates, stripes and a pseudogap are observed in MC simulations[21,22,23].

Many of these studies revealed features, e. g. an infinite compressibility near the filled lower Kondo band, which

have been interpreted as signature of PS. PS has also been reported[24] from computations based on a dynamical mean field treatment based on the DE model at $T = 0$. In previous MC studies[10,18] for the DE model with classical core spins for 1D systems, we had obtained numerical data comparable to those reported in Ref. 9,11,12. A detailed analysis of the data revealed[19] however, that the aforementioned model with the standard parameter set, relevant for the manganites, favors individual polarons over phase separation. Other authors also found ferromagnetic polarons for the almost empty lower Kondo band (i. e. very few electrons) for S=1/2 corespins[25,26], for the 1D AF Kondo Model with few electrons[27], and for the 1D paramagnet at higher temperatures[28]. In Ref. 29, small ferromagnetic droplets were predicted from energy considerations.

In this paper, we present a numerical study of the 2D ferromagnetic Kondo model with classical corespins. As in 1D, we find that the correct physical interpretation of the features which have been interpreted as PS is rather given by ferromagnetic polarons, i.e. small FM-regions with *one single* trapped charge-carrier. The polaron picture allows also a straight forward and obvious explanation of the pseudogap, which has been previously observed in the spectral density in experiments[30,31,32,33] and MC simulations[10,14]. Experimental evidence for small FM droplets in low doped $La_{1-x}Ca_xMnO_3$ is reported in Ref. 34,35.

This paper is organized as follows. In Sec. II the model Hamiltonian is presented and particularities of the MC simulation for the present model are outlined. A canonical algorithm is introduced. In Sec. III, we introduce a simplified model of ferromagnetic polarons embedded in an AFM background and present results for this model. In Sec. IV, these results are compared to unbiased Monte Carlo simulations of the 2D ferromagnetic Kondo model with classical corespins at realistic parameter values. The key results of the paper are summarized in Sec. V.

II. MODEL HAMILTONIAN AND UNBIASED MONTE CARLO

In this paper, we will concentrate solely on properties of the itinerant e_g electrons interacting with the *local* t_{2g} corespins. We also neglect the degeneracy of the e_g orbitals. The degrees of freedom of the e_g electrons are then described by a single-orbital Kondo lattice model[18]. As proposed by de Gennes[36], Dagotto *et al.*[9,14] and Furukawa[15], the t_{2g} spins $\mathbf{S}_i$ are treated classically, which is equivalent to the limit $S \to \infty$. The spin degrees of freedom ($\mathcal{S}$) are thus replaced by unit vectors $\mathbf{S}_i$, parameterized by polar and azimuthal angles θ_i and ϕ_i, respectively. The magnitude of both corespins and e_g-spins is absorbed into the exchange couplings.

A. Effective Spinless Fermions (ESF)

It is expedient to use the individual t_{2g} spin direction $\mathbf{S}_i$ as the local quantization axis for the spin of the itinerant e_g electrons at the respective sites. This representation is particularly useful for the $J_{\rm H} \to \infty$ limit, but also for the projection technique, which takes into account virtual processes for finite Hund coupling. As described in Ref. 10, the energetically unfavorable states with e_g electrons antiparallel to the local t_{2g} corespins can be integrated out. This yields the 2D effective spinless fermion model (ESF)

$$\hat{H} = -\sum_{<i,j>} t_{i,j}^{\uparrow\uparrow}\, c_i^\dagger\, c_j - \sum_{i,j} \frac{t_{i,j}^{\uparrow\downarrow}\, t_{j,i}^{\downarrow\uparrow}}{2J_{\rm H}}\, c_i^\dagger c_i + J' \sum_{<i,j>} \mathbf{S}_i \cdot \mathbf{S}_j \ . \tag{1}$$

The spinless fermion operators c_j correspond to spin-up electrons (relative to the *local* corespin-orientation) only. The spin index has, therefore, been omitted. With respect to a *global* spin-quantization axis the ESF model (1) still contains contributions from both spin-up and spin-down electrons.

The first term in Eq. (1) corresponds to the kinetic energy in tight-binding approximation. The modified hopping integrals $t_{i,j}^{\sigma,\sigma'}$ depend upon the t_{2g} corespin orientation

$$t_{i,j}^{\sigma,\sigma'} \ = \ t_0\, u_{i,j}^{\sigma,\sigma'} \ , \tag{2}$$

where the relative orientation of the t_{2g} corespins at site i and j, expressed by the angles $0 \le \vartheta \le \pi$ and $0 \le \phi < 2\pi$, enters via

$$\begin{aligned} u_{i,j}^{\sigma,\sigma}(\mathcal{S}) &= c_i c_j + s_i s_j \mathrm{e}^{i(\phi_j - \phi_i)} \quad &= \cos(\vartheta_{ij}/2)\ \mathrm{e}^{i\psi_{ij}} \\ u_{i,j}^{\sigma,-\sigma}(\mathcal{S}) &= c_i s_j \mathrm{e}^{-i\phi_j} + s_i c_j \mathrm{e}^{-i\phi_i} \quad &= \sin(\vartheta_{ij}/2)\ \mathrm{e}^{i\chi_{ij}} \end{aligned} \tag{3}$$

with the abbreviations $c_i = \cos(\vartheta_i/2)$ and $s_i = \sin(\vartheta_i/2)$. These factors depend on the relative angle ϑ_{ij} of corespins $\mathbf{S}_i$ and $\mathbf{S}_j$ and on some complex phases ψ_{ij} and χ_{ij}. For certain spin structures, an electron may obtain a different phase depending on the path taken from one lattice site to another. An example of such structures is the so called Flux phase[20,37,38].

The second term in Eq. (1) accounts for virtual hopping processes to antiparallel spin–corespin configurations and vanishes in the limit $J_{\rm H} \to \infty$. The ESF model thus takes into account virtual hopping resulting from finite $J_{\rm H}$ in the Kondo model in a similar manner as the tJ-model includes virtual hopping for finite U in the Hubbard model. The last term is a small antiferromagnetic exchange of the corespins.

The hopping strength t_0 will serve as our unit of energy. $J_{\rm H}$ is usually taken to be of the order of magnitude of $4t_0$ to $8t_0$, and J' of the order of $t_0/100$.

B. Grand Canonical Treatment

We define the grand canonical partition function as

$$\begin{aligned} \mathcal{Z}(\mu) &= \int \mathcal{D}[\mathcal{S}] \;\; \mathrm{tr}_c \, \mathrm{e}^{-\beta(\hat{H}(\mathcal{S})-\mu\hat{N})} \\ \int \mathcal{D}[\mathcal{S}] \;\; &= \prod_{i=1}^{L} \Big(\int_0^{\pi} d\theta_i \sin\theta_i \int_0^{2\pi} d\phi_i \Big) \, , \end{aligned} \tag{4}$$

where tr_c indicates the trace over fermionic degrees of freedom at inverse temperature β, $\hat{N}$ is the operator for the total number of e_g electrons and μ stands for the chemical potential. Upon integrating out the fermionic degrees of freedom, we obtain the statistical weight of a corespin configuration $\mathcal{S}$ given the chemical potential μ, which can be written as

$$w(\mathcal{S}|\mu) = \frac{\mathrm{tr}_c \, \mathrm{e}^{-\beta(\hat{H}(\mathcal{S})-\mu\hat{N})}}{\mathcal{Z}(\mu)} \, . \tag{5}$$

Equation (4) is the starting point of Monte Carlo simulations of the Kondo model[9] where the sum over the classical spins is performed via Markov chain importance sampling. The spin configurations $\mathcal{S}$ are sampled with the probability given by the weight factor $w(\mathcal{S}|\mu)$, which is computed by exact diagonalization of the corresponding one-particle Hamiltonian in Eq. (1).

Motome and Furukawa[39] suggested to replace the full diagonalization by an expansion in Chebychev polynomials. The cpu time then scales with the system size L as $O(L^2 \log(L))$ instead of $O(L^3)$ as for the full diagonalization and the algorithm can be easily parallelized. We found, however, that on single processors the full diagonalization can be accelerated to be faster than this approach up to system sizes of 10^3 lattice sites, while both algorithms would be too slow on present day's processors for larger systems. For a faster full diagonalization, the key is to exploit the structure of the Hamiltonian: The lattice sites are relabeled in order to obtain a band matrix with as few diagonals as possible. Since this is only an alternative assignment of the linear index to the two dimensional lattice vector, one does not introduce any approximation or error. Fast library routines for band matrices can then be used. Since we did parameter studies, we did not program a parallel algorithm but instead ran the whole calculation on each cpu with a different parameter set. Recently, an $O(L)$ algorithm has been proposed by the same authors, which reduces the numerical effort by approximating the matrix-vector multiplication[17].

In the 2D case we have employed MC updates in which single spins were rotated. The angle of rotation was optimized to keep the acceptance high enough. From time to time a complete flip $\mathbf{S}_i \rightarrow -\mathbf{S}_i$ was proposed. The skip between subsequent measurements was chosen to be 50 to a few hundreds of lattice sweeps reducing autocorrelations to a negligible level. We have performed MC runs with some hundreds to 2000 measurements on a 12×14 lattice. This geometry was chosen to reduce finite size (closed shell) effects observed on a square lattice. The number of measurements was higher for calculations in the polaronic regime, where the particle number fluctuates strongly, in order to have sufficient measurements for each filling.

As previously shown[18], the spin-integrated one-particle Green's function in global quantization can be written as

$$\sum_{\sigma} \ll a_{i\sigma}; a_{j\sigma}^{\dagger} \gg_{\omega} = \int \mathcal{D}[\mathcal{S}] \; w(\mathcal{S}|\mu) u_{ji}^{\uparrow\uparrow}(\mathcal{S}) \ll c_i; c_j^{\dagger} \gg_{\omega}^{\mathcal{S}} \, , \tag{6}$$

where $\ll c_i; c_j^{\dagger} \gg_{\omega}^{\mathcal{S}}$ is the Green's function in local spin quantization. It can be expressed in terms of the one-particle eigenvalues $\epsilon^{(\lambda)}$ and the corresponding eigenvectors $\psi^{(\lambda)}$ of the Hamiltonian $\hat{H}(\mathcal{S})$:

$$\ll c_i; c_j^{\dagger} \gg_{\omega}^{\mathcal{S}} = \sum_{\lambda} \frac{\psi^{(\lambda)}(i) \, \psi^{*(\lambda)}(j)}{\omega - (\epsilon^{(\lambda)} - \mu) + i0^+}$$

It should be pointed out that the one-particle density of states (DOS) is identical in global and local quantization; for details see Ref. 18.

C. Canonical Algorithm

Since there is a jump in the electron density at the critical chemical potential (shown later in Fig. 5), some electron fillings cannot be examined with the grand canonical algorithm, and we therefore developed a canonical scheme. In Ref. 20, canonical calculations were done by computing the eigenenergies for each corespin configuration and then filling the available electrons into the lowest levels. This method does, however, not account for thermal particle-hole excitations around the Fermi energy. When several states have similar energy, these may become important.

On the other hand, an exact approach would mean calculating the Boltzmann weight for every possible distribution of N_{el} particles on L energy levels and summing over their contributions. Even for small lattice sizes L, this clearly becomes too demanding for more than a few electrons or holes. Instead, we took into account just the lowest excitations of the Fermi sea by filling $N_{el}^0 < N_{el}$ electrons into the N_{el}^0 lowest states and considering only the distributions of the $N_{el} - N_{el}^0$ remaining electrons on the states around the Fermi energy. Usually, it is sufficient to take $N_{el} - N_{el}^0 \approx 5$. The weight for the corespin configuration $\mathcal{S}$ then depends on the particle number instead of the chemical potential:

$$w(\mathcal{S}|N_{el}) = \frac{\sum_{\tilde{\mathcal{P}}} \mathrm{e}^{-\beta \hat{H}(\mathcal{S}, \tilde{\mathcal{P}}(N_{el}))}}{\mathcal{Z}(N_{el})} \, , \tag{7}$$

where $\tilde{\mathcal{P}}$ denotes these restricted permutations.

Although this is more time-consuming than the grand canonical calculation of the fermionic weight, the additional consumption of computer time is small compared to the time needed for the diagonalization of the one-particle Hamiltonian. The particle-hole excitations, which are thus included, can be crucial when examining competition between phases with and without a pseudogap.

A MC update - especially a complete spin flip - may lead to a configuration which is very unlikely to occur at the given particle number, although it may be a good configuration for a different filling. A later MC move might then lead back to the original particle number, and these moves should improve autocorrelation. We therefore allow density fluctuations within a set of four to five particle numbers. In order to spend a comparable number of MC steps at each filling, prior weight factors $g(N_{el})$ were introduced and adjusted in a prerun, giving

$$w(\mathcal{S}) = \sum_{N_{el}=N_{min}}^{N_{max}} w(\mathcal{S}|N_{el}) \cdot g(N_{el}) \; . \tag{8}$$

The sum is taken over the set of allowed particle numbers $N_{min} \leq N_{el} \leq N_{max}$ and $w(\mathcal{S}|N_{el})$ is calculated according to eq. 7.

When evaluating observables for fixed electron number, one has to calculate the expectation value

$$\langle \, \mathcal{O} \, \rangle_{N_{el}} = \frac{\sum_{\mathcal{S}} \mathcal{O}(\mathcal{S})_{N_{el}} \cdot w(\mathcal{S}|N_{el})}{\sum_{\mathcal{S}} w(\mathcal{S}|N_{el})} \; , \tag{9}$$

which can be rewritten as

$$\langle \, \mathcal{O} \, \rangle_{N_{el}} = \frac{\sum_{\mathcal{S}} \mathcal{O}(\mathcal{S})_{N_{el}} \frac{w(\mathcal{S}|N_{el})}{w(\mathcal{S})} \cdot w(\mathcal{S})}{\sum_{\mathcal{S}} \frac{w(\mathcal{S}|N_{el})}{w(\mathcal{S})} \cdot w(\mathcal{S})} \; , \tag{10}$$

Configurations $\mathcal{S}$ occur in the Markov Chain with probability proportional to $w(\mathcal{S})$; when the sum is taken over the configurations produced by the MC run, the expectation value therefore becomes

$$\langle \, \mathcal{O} \, \rangle_{N_{el},\, MC} = \frac{\sum_{\mathcal{S},MC} \mathcal{O}(\mathcal{S})_{N_{el}} \frac{w(\mathcal{S}|N_{el})}{w(\mathcal{S})}}{\sum_{\mathcal{S},MC} \frac{w(\mathcal{S}|N_{el})}{w(\mathcal{S})}} \; . \tag{11}$$

III. FERROMAGNETIC POLARON MODEL

Near half filling of a single e_g band, a tendency toward phase separation has been reported in various computational studies[9,11,12,24].

In most cases, the existence of phase separation is inferred from a discontinuity of the electron density as a function of the chemical potential. At the critical chemical potential where this discontinuity is found, it is claimed that the system separates into FM domains of high carrier concentration and AFM domains of low carrier concentration.

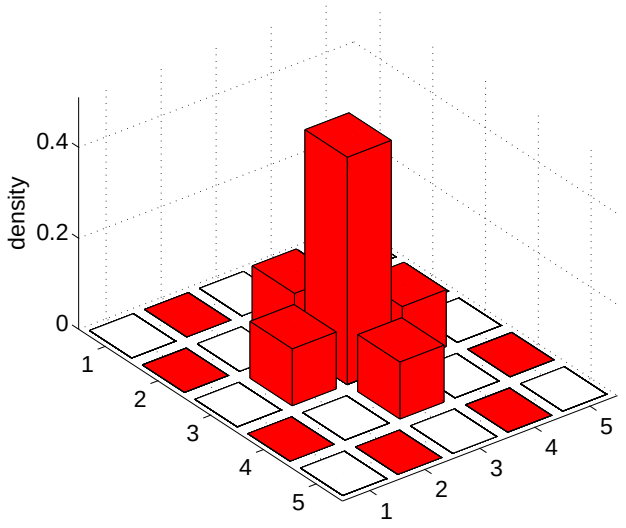

FIG. 1: Idealized spin and hole-density configuration for the groundstate of a FM polaron of $L_{\rm f} = 5$ lattice sites, embedded in an AFM background. Empty (filled) squares represent spin down (up). Height represents hole density.

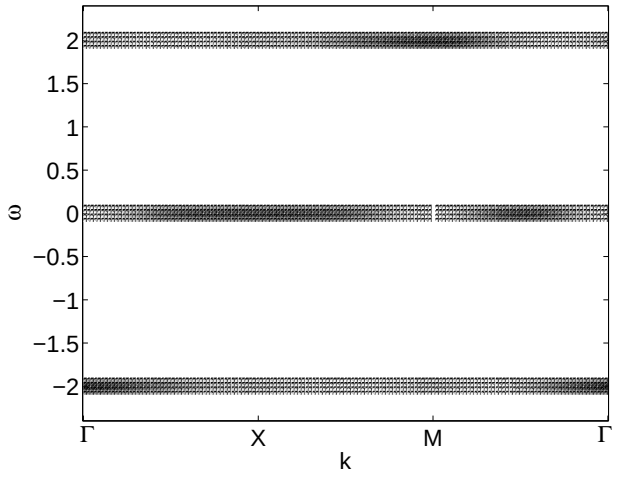

FIG. 2: Contribution of the idealized ferromagnetic polaron to the one-particle spectral function. For visibility, the δ-peaks have been broadened to a width of 0.2.

We have already shown that for a 1D system this picture is in general incorrect[19]. In fact, what happens is that each single hole is dressed by a ferromagnetic cloud in which it delocalizes. The system can be well described by free quasiparticles consisting of a single hole plus a local (three to four-sites for 1D, 5 sites for 2D) ferromagnetic well embedded in an AF background. Each of these added quasiparticles gains the same energy, which is exactly balanced by the energy to be paid for the critical chemical potential μ^*. Hence the discontinuity of the particle number at low temperatures.

Here we show that ferromagnetic polarons, i.e. *single* charge carriers surrounded by small ferromagnetic spin-

clouds, are indeed formed when holes are doped into a completely filled lower Kondo band in 2D. In this section we discuss the properties of idealized two dimensional model polarons, whereas in the next section we compare our polaron-model to unbiased Monte Carlo results.

A. One single polaron

As reference configuration we consider the completely filled lower Kondo band where super exchange and the contribution from the virtual hopping process, see Eq. (1), give rise to an antiferromagnetic corespin pattern. The smallest defect in a completely antiferromagnetically ordered 2D lattice is the flipping of one single spin. Then a five-site ferromagnetic region forms. If we introduce a hole into the system, it can delocalize in this region because of the double-exchange mechanism. As there is no double-exchange hopping between sites with perfectly antiferromagnetic spins, the hole is trapped inside the ferromagnetic region. In this simple model, the hole can hop from the central site of this region (site 1) where the spin has been flipped, to all nearest neighbors (sites 2–5). The tight-binding Hamiltonian describing this situation reads

$$H_{\rm hole} = -t_{\rm f} \begin{pmatrix} 0 & 1 & 1 & 1 & 1 \\ 1 & 0 & 0 & 0 & 0 \\ 1 & 0 & 0 & 0 & 0 \\ 1 & 0 & 0 & 0 & 0 \\ 1 & 0 & 0 & 0 & 0 \end{pmatrix} ,$$

with the hopping between ferromagnetic sites $t_{\rm f}$ in this model. Since the Hamiltonian is symmetric with respect to rotations by $\pi/2$, the ground state should also show this property and can thus be found in the space spanned by $(1,0,0,0,0), (0,1/2,1/2,1/2,1/2)$, where the Hamiltonian reads

$$H_{\rm hole} = -t_{\rm f} \begin{pmatrix} 0 & 2 \\ 2 & 0 \end{pmatrix} .$$

The delocalization energy of the hole is thus given by $\epsilon_{hole} = -2\,t_{\rm f}$. This energy can be gained as a hole delocalizes in the ferromagnetic domain. The ground state $1/\sqrt{2}\ (1,1/2,1/2,1/2,1/2)$ has the hole density depicted in Fig. 1. Excited states are found at $\epsilon = +2\,t_{\rm f}$ and $\epsilon = 0$. The highest state at $\epsilon = +2\,t_{\rm f}$ is given by $1/\sqrt{2}\ (-1,1/2,1/2,1/2,1/2)$ and does also have s-symmetry, while the states at $\epsilon = 0$ have p- and d-symmetry. They appear in the one-particle spectral function of the configuration shown in Fig. 2.

To create such a ferromagnetic domain, however, four antiferromagnetic bonds have to be broken. This costs the energy of $2 \times 4\,J_{\rm eff}$. Near the completely filled lower Kondo band $x = 0$, the total antiferromagnetic exchange coupling is approximately given by $J_{\rm eff} = 1/(2J_H) + J'$, see Ref. 19. The energy gained by adding one hole to the system thus reads

$$\epsilon_{\rm pol} = -2\,t_{\rm f} + 8J_{\rm eff} \qquad (12)$$

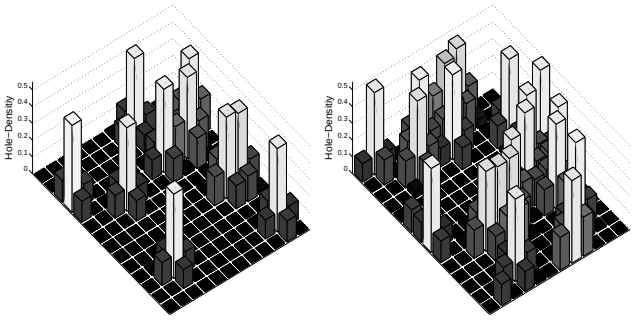

FIG. 3: Representative hole-density configuration for 10 (left) and 20 (right) holes in the simplified polaron model on a 12×14 lattice ($x \approx 0.12$). The holes are located where one spin is flipped from the AFM reference configuration. The results correspond to $\beta = 50$, $J' = 0.02$, $J_H = 6$. Colors are for better visibility.

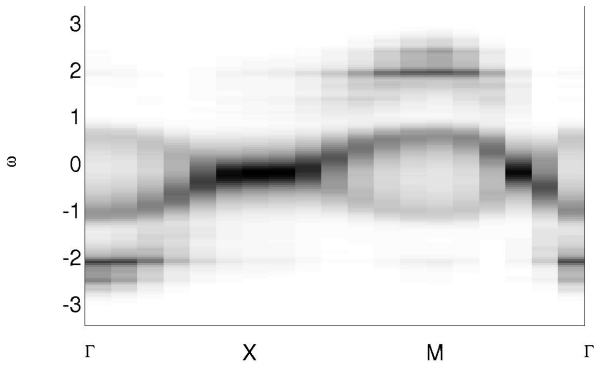

FIG. 4: Spectral density of the polaron model for 20 holes on a 12×14 lattice ($x \approx 0.12$), using the same parameter values as Fig. 3.

When the chemical potential approaches $-\epsilon_{\rm pol}$ from above, holes start to enter the system forming individual polarons. Therefore, the critical chemical potential is given by $\mu^* = -\epsilon_{\rm pol}$.

Up to a certain concentration, these holes can be treated as free fermions which all have the same energy $\epsilon_{\rm pol}$. The energy may, however, depend on the temperature if $t_{\rm f}$ or $J_{\rm eff}$ do. The more obvious temperature effect is the smearing of the discontinuity in the electron filling at higher temperatures, which results from the application of the Fermi-Dirac statistics to these quasiparticles.

B. Results for a small number of polarons

In this subsection we push our polaron ideas further to treat the case of a small number of holes in an AFM background. To this end, we perform a simple simulation. We start with a perfect AFM reference configuration. We then add $N_{\rm holes}$ holes by flipping $N_{\rm holes}$ randomly chosen spins, excluding flipping a spin back. Finally, we add random deviations to each corespin in

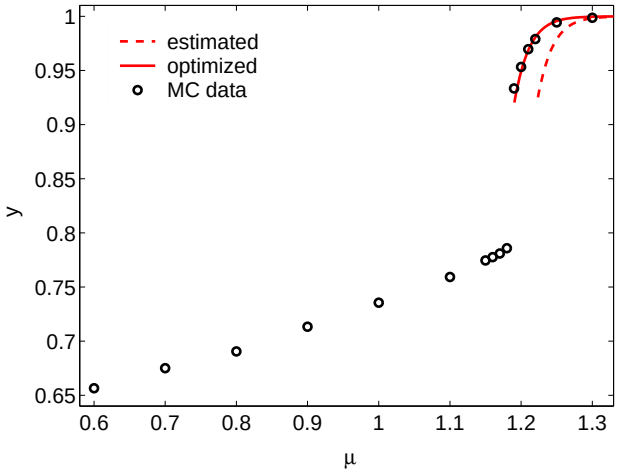

FIG. 5: Electron density y as a function of the chemical potential μ of a 14×12 lattice for $\beta = 50$, $J' = 0.02$ and $J_{\rm H} = 6$. Circles indicate MC results, the solid (dashed) line shows the free fermion results for the fitted (estimated) energy.

order to account for thermodynamic fluctuations. These fluctuations lead to a finite DE hopping amplitude in the AFM band and their size is therefore fitted to match the bandwidth observed in the MC results, see sec. IV. We then diagonalize the resulting ESF-Hamiltonian and compute observables in the canonical ensemble with $N_{\rm el} = N_{\rm sites} - N_{\rm holes} = N_{\rm sites} - N_{\rm flipped\ spins}$ as explained in sec. II C. The observables are averaged over many such configurations. Typical hole-density configurations are depicted in Fig. 3 for 10 and 20 holes, i. e. 10 resp. 20 spins were flipped from the initial perfect AF configuration. In the formulae for the ESF-Hamiltonian and the observables, the parameters were set to $\beta = 50$, $J' = 0.02$ and $J_H = 6$. It should be emphasized that the probability distribution used in choosing the spins to be flipped is completely flat. It is only ensured that exactly $N_{\rm holes}$ spins are flipped from the AFM reference configuration. The chosen parameter values therefore do not influence the obtained spin configurations.

As an example for observables calculated in this pure polaron model, we show the one-particle spectral function for 20 holes in Fig. 4. The center is occupied by the AFM tight-binding band with a mirror band due to the doubling of the unit cell in the AFM spin configuration. At $\omega = \pm 2$, the polaronic states can be clearly seen. In addition to them, one sees a number of weaker signals in the vicinity of $\omega = \pm 2$. These stem from larger ferromagnetic regions, i. e. from contiguous polarons.

IV. UNBIASED MC RESULTS

In this section we present results of unbiased Monte Carlo simulations for $J' = 0.02$ and $J_{\rm H} = 6$ and show that they correspond to independent ferromagnetic polarons.

Figure 5 shows the electron density as a function of the chemical potential at $\beta = 50$. Depending on the value of the hopping parameter t_0, this is in a range of $50K - 100K$, i. e. relevant for experiments. There is a discontinuity in the density (infinite compressibility), but one observes that the electron number does not drop at once from 1 (AFM) to 0.8 (FM). Instead, it first decreases only slowly from the completely filled band, the slope of the curve then becomes gradually steeper until it is vertical. For a qualitative description of the MC results by the polaron model, we use $t_{\rm f} = t_0$ and $J_{\rm eff} = 1/(2J_H) + J'$ which yields a polaron energy of $\epsilon_{\rm pol} \simeq -1.17$. Using this value for the critical chemical potential we obtain the dashed line. Although it is shifted by some constant energy, it already correctly reflects the trend in the Monte Carlo data. Much better agreement can be found by fitting the polaron energy to the Monte Carlo data. In our case we obtain $\epsilon_{\rm pol} \simeq -1.14$. The corresponding Fermi function is shown as the solid line.

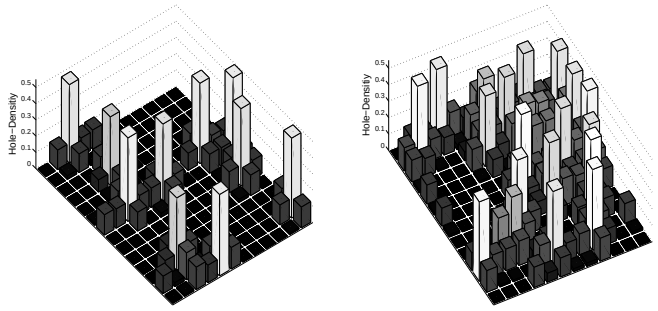

FIG. 6: MC snapshot of the hole density for 10 (left) resp. 20 (right) holes in a 14×12 lattice at $\beta = 50$, $J' = 0.02$, $J_H = 6$.

Fig. 6 shows MC snapshots with 10 and 20 holes.The polarons can be clearly seen, 10 polarons for 10 holes and 19 polarons for 20 holes. Only the 20^{th} hole at the larger doping is delocalized. There is an obvious similarity to the idealized polaron model, see Fig. 3.

As in the one-dimensional case, the polarons induce separate states in the one-particle density of states (DOS), as described in sec. III. Figure 7 shows the DOS in the case of one hole in a 14×12 lattice at various temperatures. One observes a broad peak in the center and two polaronic peaks at ± 2 that are separated by a pseudogap. The pseudogap observed in the Kondo model is thus a direct result of the FM polarons. The broad central peak is due to holes moving in the not quite perfectly antiferromagnetic background. As a result of the super exchange term in the Hamiltonian, it is centered around $\epsilon = -z/(2J_{\rm H})$ with $z = 4$ in the 2D square lattice. When no hole is in the system, this peak also shows up and is then the only feature of the DOS. The width of the peak is mainly dominated by corespin fluctuations around the completely ordered state. Consequently the width decreases with decreasing temperature. This leads to a wider pseudogap at lower temperatures, as depicted in Fig. 7.

The polaronic peak, on the other hand, remains largely

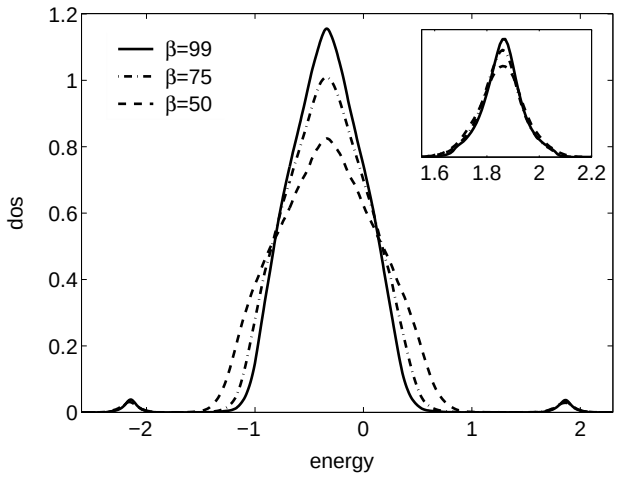

FIG. 7: Temperature-dependence of the one-particle DOS in the case of one hole in a 14×12 lattice, $J' = 0.02, J_{\rm H} = 6$. The inset shows an enlargement of the polaronic peak.

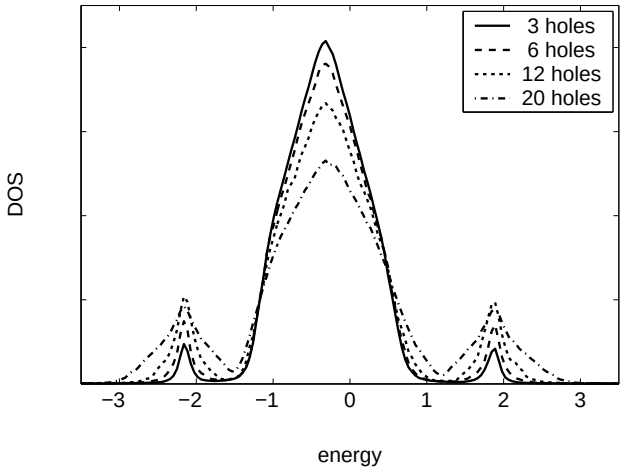

FIG. 8: Doping dependence of the one-particle DOS for $J' = 0.02$, $\beta = 50$, $J_{\rm H} = 6$.

unaffected by temperature. As can be seen in the inset of Fig. 7, its shape is virtually constant. Upon introducing more holes (see Fig. 8), the weight of the polaronic peaks increases whereas their position and the shape of the central band remain unaffected. The weight of the polaronic peaks corresponds to the number of holes. The shape of both the antiferromagnetic band and the polaronic peaks only begins to change when a large number of holes are added, so that the probability for overlapping polarons becomes considerable. With 5 sites per polaron, 20 polarons would take 100 sites, or 60% of a 14×12 lattice, therefore connected polarons and disturbances of the AF background are to be expected. It is therfore impressive that even with 20 holes, the polarons seem to remain largely independent.

Fig. 9 shows the spectral density for the ESF model

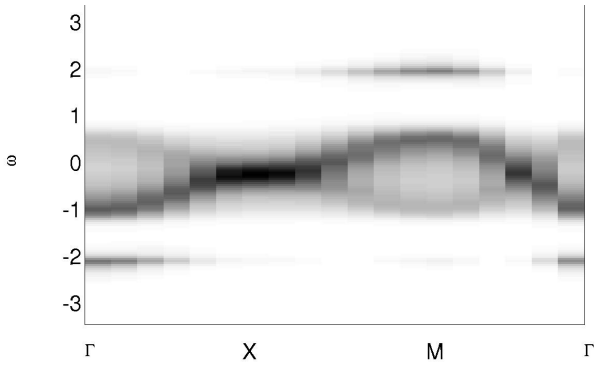

FIG. 9: Spectral density for $J' = 0.02, \beta = 50$, $J_{\rm H} = 6$ and six holes ($x \approx 0.035$) on a 12×14 lattice: Polaronic states in addition to the AFM band.

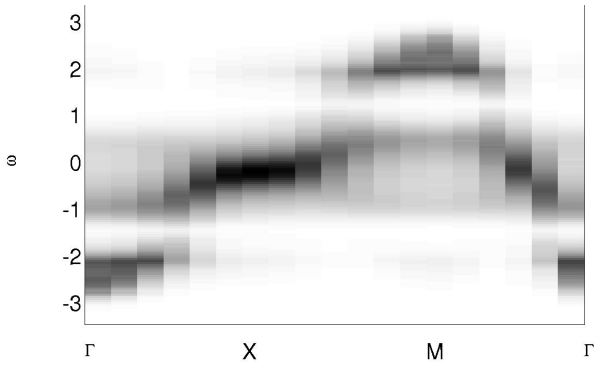

FIG. 10: Spectral density for $J' = 0.02$, $\beta = 50$, $J_{\rm H} = 6$ and 20 holes ($x \approx 0.12$) on a 12×14 lattice.

with $J_{\rm H} = 6$, $J' = 0.02$, $\beta = 50$ and 6 holes. In addition to the central band, the polaronic states can be seen at energies slightly below ± 2, in perfect agreement with the simple polaron model, see Fig. 2. The states at $\omega \approx 0$ are lost within the AFM band. Fig. 10 shows the results for 20 holes ($x \approx 0.12$). Compared to the results for the simple polaron model in Fig. 4, the structures are slightly smeared, but the similarities are striking.

In order to verify that the addition of holes leads primarily to more small polarons rather than to a growth of the existing ones, we use a dressed corespin correlation function

$$S_h(\vec{r}) = \frac{1}{L} \sum_{\vec{i}} n^h_{\vec{i}} S_{\vec{i}} \cdot S_{\vec{i}+\vec{r}} \,. \tag{13}$$

Where $n^h_{\vec{i}}$ is the hole density at site $\vec{i}$ related to the electron density via $n^h_{\vec{i}} = 1 - n_{\vec{i}}$, the sum over $\vec{i}$ is taken over all lattice sites. This dressed correlation measures the ferromagnetic regions around holes. Fig. 11 shows the results for 1, 6 and 20 holes on 12×14 sites, which correspond to doping levels of $x = 0.006$, $x = 0.036$, and $x = 0.12$. The results are almost independent of the doping level x and, above all, the ferromagnetic region does not grow with increasing hole density. The data

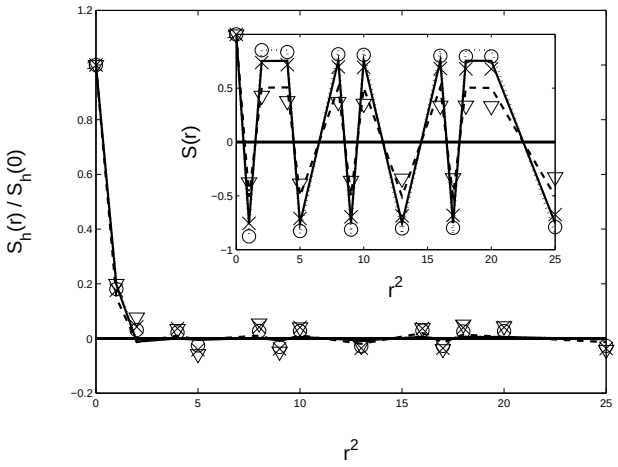

FIG. 11: Dressed corespin correlation Eq. (13) for $J' = 0.02$ from unbiased MC Data for 1 ($\circ$), 6 ($\times$) and 20 ($\triangledown$) holes. Continuous lines are data for the simple Polaron model (see sec. III): 1 Polaron (dotted), 6 (solid) and 20 Polarons (dashed). The inset shows the corespin correlation $S(\vec{r}) = \frac{1}{L}\sum_{\vec{i}} S_{\vec{i}} \cdot S_{\vec{i}+\vec{r}}$. The MC Simulations were done for $J_{\rm H} = 6$, $\beta = 50$ on a 12×14 lattice.

are compared to those obtained for the independent polaron model introduced in sec. III and show very good agreement. The inset of Fig. 11 shows the usual corespin correlation which reveals the AFM background. The antiferromagnetism decreases with increasing hole concentration, both for the MC simulations and the idealized polaron model. However, it shrinks somewhat faster for the full ESF model.

The MC results for 1 and 6 holes were obtained from a grand canonical simulation evaluated in subspaces with constant particle number; the results for 20 holes were calculated with the canonical algorithm introduced in sec. II C, because this doping can not be stabilized in the grand canonical ensemble, see Fig.5.

V. CONCLUSIONS

In this paper, the ferromagnetic Kondo (double-exchange) model in 2D has been analyzed by unbiased finite temperature Monte-Carlo simulations. It has been found that upon hole doping, small ferromagnetic regions appear around each individual hole while the rest of the lattice stays antiferromagnetically ordered. Each of the ferromagnetic regions contains one single hole. Therefore, the physics close to half filling is not governed by phase separation into larger FM and AF regions, as previously reported, but by single-hole ferromagnetic polarons moving in an antiferromagnetic background.

The critical chemical potential μ^* at which holes start to enter the lower Kondo band can be found from simplified energy considerations (Eq. (12)). For μ significantly above μ^*, the band is completely filled and the corespins are antiferromagnetic. Around μ^*, holes enter the e_g-band, forming isolated FM domains in the shape depicted in Fig. 1, each containing one *single* hole. This is corroborated by MC snapshots, the functional dependence of the electron density on the chemical potential, the spectral density and the dressed corespin correlation Eq. (13).

The discontinuity in the electron density vs. the chemical potential (i. e. infinite compressibility) is usually taken as evidence for PS. In the case of the Kondo model, this discontinuity is a consequence of a large (macroscopic) number of degenerate polaron states. When the chemical potential is close to the energy of these states, the number of holes (polarons) in the lattice strongly fluctuates. The weight of the polaron peak in the spectrum is directly linked to the number of holes (Fig. 8). In order to obtain numerical results at a fixed hole number, it was necessary to develop a canonical algorithm for our Monte Carlo simulations.

Another consequence of the formation of single-hole FM polarons is the opening of a pseudogap. The small FM regions of the polarons contain only a few electronic states that are energetically well separated from each other. Moreover, the width of the antiferromagnetic band is much smaller than the difference between the highest and the lowest polaron states. Therefore, no states can be found for energies between the upper edge of the antiferromagnetic band and the highest state within the polaron. This gives rise to a pseudogap in the one-particle spectral function. The same arguments explain the apprearance of a mirror gap well below the chemical potential.

A pseudogap is indeed observed in experiments[30,31,32] and in MC simulations for the Kondo model[10,14]. If there were larger FM clusters, however, they would give rise to additional states at the energies of the pseudogap. The gap would disappear. Experiments at low doped $La_{1-x}Ca_xMnO_3$ showed evidence of small FM droplets in an AFM background[34,35].

Our analysis yields compelling evidence against the PS scenario and in favor of FM polarons in 2D for realistic parameter values for manganites. A similar behavior has been previously found for 1D. Furthermore, the coupling to lattice degrees of freedom will additionally localize holes and inhibit the formation of a ferromagnetic phase (Jahn-Teller polarons)[6,40]. It should be noted that, depending on the value of the hopping parameter t_0, the temperature investigated in this paper ($\beta = 50$) is in a range of $50K - 100K$, which is in agreement with temperatures in experiments.

VI. ACKNOWLEDGMENTS

This work has been supported by the Austrian Science Fund (FWF), project no. P15834-PHY. We wish to thank the EPSRC (Grant GR/S18571/01) for financial support.

* Electronic address: daghofer@itp.tu-graz.ac.at

[1] T. Kaplan and S. Mahanti, *Physics of Manganites* (Kluwer Academic/ Plenum Publishers, New York, Boston, Dordrecht, London, Moscow, 1998), 1st ed.

[2] E. L. Nagaev, *Colossal Magnetoresistance and Phase Separation in Magnetic Semiconductors* (Imperial College Press, London, 2002), 1st ed.

[3] P. Horsch, J. Jaklic, and F. Mack, Phys. Rev. B **59**, R14149 (1999).

[4] J. Bala, A. M. Oles, and P. Horsch, Phys. Rev. B **65**, 134420/1 (2002).

[5] C. Zener, Phys. Rev. **82**, 403 (1951).

[6] D. M. Edwards, Adv. Phys. **51**, 1259 (2002).

[7] D. Meyer, C. Santos, and W. Nolting, J. Phys. Condens. Matter **13**, 2531 (2001).

[8] W. Müller and W. Nolting, Phys. Rev. B **66**, 085205 (2002).

[9] E. Dagotto, S. Yunoki, A. L. Malvezzi, A. Moreo, J. Hu, S. Capponi, D. Poilblanc, and N. Furukawa, Phys. Rev. B **58**, 6414 (1998).

[10] W. Koller, A. Prüll, H. G. Evertz, and W. von der Linden, Phys. Rev. B **66**, 144425 (2002).

[11] S. Yunoki and A. Moreo, Phys. Rev. B **58**, 6403 (1998).

[12] S. Yunoki, J. Hu, A. L. Malvezzi, A. Moreo, N. Furukawa, and E. Dagotto, Phys. Rev. Lett. **80**, 845 (1998).

[13] H. Yi, N. H. Hur, and J. Yu, Phys. Rev. B **61**, 9501 (2000).

[14] E. Dagotto, T. Hotta, and A. Moreo, Phys. Rep. **344**, 1 (2001).

[15] N. Furukawa, *in: Physics of manganites* (Kluwer Academic Publisher, New York, 1998), 1st ed.

[16] Y. Motome and N. Furukawa, J. Phys. Soc. Jpn. **69**, 3785 (2000).

[17] Y. Motome and N. Furukawa, J. Phys. Soc. Jpn. **72**, 2126 (2003).

[18] W. Koller, A. Prüll, H. G. Evertz, and W. von der Linden, Phys. Rev. B **67**, 104432 (2003).

[19] W. Koller, A. Prüll, H. G. Evertz, and W. von der Linden, Phys. Rev. B **67**, 174418 (2003).

[20] H. Aliaga, B. Normand, K. Hallberg, M. Avignon, and B. Alascio, Phys. Rev. B **64**, 024422 (2001).

[21] M. Moraghebi, C. Buhler, S. Yunoki, and A. Moreo, Phys. Rev. B **63**, 214513 (2001).

[22] M. Moraghebi, S. Yunoki, and A. Moreo, Phys. Rev. B **66**, 214522 (2002).

[23] M. Moraghebi, A. Moreo, and S. Yunoki, Phys. Rev. Lett. **88**, 187001 (2002).

[24] A. Chattopadhyay, A. J. Millis, and S. Das Sarma, Phys. Rev. B **64**, 012416 (2001).

[25] C. D. Batista, J. Eroles, M. Avignon, and B. Alascio, Phys. Rev. B **58**, 14689 (1998).

[26] C. D. Batista, J. Eroles, M. Avignon, and B. Alascio, Phys. Rev. B **62**, 15047 (2000).

[27] G. Homer and M. Gulacsi, Journal of Superconductivity **12**, 237 (1999).

[28] H. Aliaga, M. T. Causa, M. Tovar, and B. Alascio, Physica B **320**, 75 (2002).

[29] M. Yu Kagan, A. V. Klapstov, I. V. Brodsky, K. I. Kugel, A. O. Sboychakov, and A. L. Rakhmanov, J. Phys. A: Math. Gen. **36**, 9155 (2003).

[30] D. S. Dessau, T. Saitoh, C. H. Park, Z. X. Shen, P. Villella, N. Hamada, Y. Moritomo, and Y. Tokura, Phys. Rev. Lett. **81**, 192 (1998).

[31] T. Saitoh, D. S. Dessau, Y. Moritomo, T. Kimura, Y. Tokura, and N. Hamada, Phys. Rev. B **62**, 1039 (2000).

[32] Y.-D. Chuang, A. D Gromko, D. S. Dessau, T. Kimura, and Y. Tokura, Science **292**, 1509 (2001).

[33] J.H. Park, C. T. Chen, S-W. Cheong, W. Bao, G Meigs, V. Chakarian, and Y. U. Idzerda, Phys. Rev. Lett **76**, 4215 (1996).

[34] G. Biotteau, M. Hennion, J. Rodriguez-Cervajal, L. Pinsard, and A. Revcolevschi, Phys. Rev. B **64**, 104421 (2001).

[35] M. Hennion, F. Moussa, G. Biotteau, J. Rodriguez-Cervajal, L Pinsard, and A. Revcolevschi, Phys. Rev. Lett. 81 **81**, 1957 (1998).

[36] P.-G. de Gennes, Phys. Rev. **118**, 141 (1960).

[37] D. F. Agterberg and S. Yunoki, Phys. Rev. B **62**, 13816 (2000).

[38] M. Y. W. Koshibae and S. Maekawa, Phys. Rev. Lett. **81**, 5604 (1998).

[39] Y. Motome and N. Furukawa, J. Phys. Soc. Jpn. **68**, 3853 (1999).

[40] A. J. Millis, R. Mueller, and B. I. Shraiman, Phys. Rev. B **54**, 5389 (1996).